Distribution of lipids in non-lamellar phases of their mixtures

Xiao-jun Li and M. Schick
Department of Physics, Box 351560
University of Washington, Seattle 98195-1560
(December 30, 1999)

We consider a model of lipids in which a head group, characterized by its volume, is attached to two flexible tails of equal length. The phase diagram of the anhydrous lipid is obtained within self-consistent field theory, and displays, as a function of lipid architecture, a progression of phases: body-centered cubic, hexagonal, gyroid, and lamellar. We then examine mixtures of an inverted hexagonal forming lipid and a lamellar forming lipid. As the volume fractions of the two lipids vary, we find that inverted hexagonal, gyroid, or lamellar phases are formed. We demonstrate that the non-lamellar forming lipid is found preferentially at locations which are difficult for the lipid tails to reach. Variations in the volume fraction of each type of lipid tail are on the order of one to ten per cent within regions dominated by the tails. We also show that the variation in volume fraction is correlated qualitatively with the variation in mean curvature of the head-tail interface.

I. INTRODUCTION

The lipid bilayer which provides the basic structure of biological membranes is composed of a large number of different lipids, of which many, on their own, form non-lamellar phases. Just what role these non-lamellar forming lipids play in the properties of membranes has been the subject of much speculation[1–3]. That they serve important functions is indicated by the fact that cells with common lipids regulate their composition to maintain a proper balance between those that form lamellar phases and those that do not[4]. At least two major roles for non-lamellar forming lipids have been proposed. One is that, because such lipids are characterized by tails which tend to splay outward, their presence alters the pressure profile within a bilayer permitting embedded proteins to function[5]. The second, noting that the lipid balance referred to above is close to a lamellar non-lamellar phase transition[4,6], posits that these lipids with their splaying tails may serve to facilitate the formation of structures not unlike the non-lamellar phases, structures which are characterized by volumes which are difficult for other lipid tails to fill, or regions of non-zero curvature. In this way they could stabilize transient fusion intermediates. For example, some scenarios of membrane fusion involve the formation of a thin cylindrical stalk[7–9] created from the lipids of the opposing leaves of the bilayers. Such a structure has a non-zero curvature, and creates regions surrounding it which are difficult for the tails to fill[8]. By concentrating in such regions, non-lamellar forming lipids could make such structures, and the processes they bring about, less costly[8,10]. In a series of experiments, Gruner and co-workers have shown that inverted hexagonal, H_{II}, phases which are characterized by periodic regions which are difficult to fill can be stabilized by the addition of alkanes[11]. Presumably the alkanes are found preferentially in these regions and lower the free energy to form these structures. Theoretical confirmation of this idea in the somewhat analogous system of block copolymer and homopolymer mixtures was provided by Matsen[12]. Tate and Gruner[13] further showed that the addition of small amounts of long chain (two tails of 22 or 24 carbons) phosphatidylcholine to dioleoylphosphatidylethanolamine (two tails of 18 carbons) stabilized the H_{II} phase relative to that produced by the addition of phosphatidylcholine with two shorter tails of 18 carbons. This provided further indirect evidence for the common hypothesis that difficult to fill, "frustrated" volumes and/or regions of high curvature[14] should be correlated with a density difference between lamellar- and non lamellar-forming lipids. However there appears to be neither experimental evidence nor theoretical calculations that directly bear on this hypothesis, or provide an indication of the magnitude of the variation in density of the different lipids. It is the purpose of this paper to demonstrate and to quantify, in a model lipid mixture, this variation of density of the lamellar- and non lamellar-forming lipids in inverted hexagonal, H_{II}, and gyroid ($Ia3d$) phases.

Our paper is organized as follows. In section II, we present the model of the lipids and develop the self consistent field theory in real space. In section III we develop the self consistent field theory in Fourier space. In section IV(A) we present our results for the phase diagrams of the single lipid as a function of its architecture, and for the anhydrous mixture of a lamellar forming and a non-lamellar forming lipid. We also show that there exists an "effective single lipid approximation" by which the latter phase diagram can be obtained from the former. In section IV(B) we present our results for the variation of the densities of the two lipids in the lamellar, inverted hexagonal, and gyroid phases. This

variation is on the order of 1 to 10%. We also compare qualitatively this variation with that of the mean curvature of the structures.

II. THEORY: REAL SPACE

The model which we employ has been presented elsewhere[15], so we will be brief here. We consider an anhydrous mixture of n_1 lipids of type 1 and n_2 lipids of type 2. Below we shall choose their architecture so that type 1 lipids form lamellar phases while type 2 lipids form H_{II} phases. All lipids consist of the *same* head group of volume v_h and two equal-length tails. Thus we model mixtures of lipids drawn from a homologous series, such as the phosphatidylethanolamines studied by Seddon et al.[16]. Each tail of lipid 1 consists of N_1 segments of volume v_t, while those of lipid 2 consist of N_2 such segments. For convenience, we denote $N_L = N\alpha_L$ for $L = 1, 2$. The tails are treated as being completely flexible, with radii of gyration $R_{g,L} = (N_L a^2/6)^{1/2}$ for each tail. The statistical segment length is a. The configuration of the l'th lipid of type L is described by a space curve $\mathbf{r}_{l,L}(s)$ where s ranges from 0 at one end of one tail, through $s = \alpha_L/2$ at which the head is located, to $s = \alpha_L$, the end of the other tail. The system is completely described by the dimensionless densities of the head groups $\hat{\Phi}_h^{(L)}(\mathbf{r})$ and of the tail segments, $\hat{\Phi}_t^{(L)}(\mathbf{r})$, which can be written

$$\hat{\Phi}_h^{(L)}(\mathbf{r}) = v_h \sum_{l=1}^{n_L} \delta\left(\mathbf{r} - \mathbf{r}_{l,L}(\alpha_L/2)\right), \tag{1}$$

$$\hat{\Phi}_t^{(L)}(\mathbf{r}) = v_h \sum_{l=1}^{n_L} \int_0^{\alpha_L} \delta\left(\mathbf{r} - \mathbf{r}_{l,L}(s)\right) ds, \tag{2}$$

where v_h has been chosen as a convenient volume to make all densities dimensionless. The number density of tail segments of type L is $(2N/v_h)\hat{\Phi}_t^{(L)}$, and their volume fraction is $(2Nv_t/v_h)\Phi_t^{(L)} \equiv \gamma_t \Phi_t^{(L)}$. The sole explicit interaction in the system is between head and tail segments, and this interaction energy E takes the form

$$\frac{1}{kT}E[\hat{\Phi}_h^{(1)} + \hat{\Phi}_h^{(2)}, \hat{\Phi}_t^{(1)} + \hat{\Phi}_t^{(2)}] \equiv \frac{2N\chi}{v_h} \int \left[\hat{\Phi}_h^{(1)}(\mathbf{r}) + \hat{\Phi}_h^{(2)}(\mathbf{r})\right] \left[\hat{\Phi}_t^{(1)}(\mathbf{r}) + \hat{\Phi}_t^{(2)}(\mathbf{r})\right] d\mathbf{r}, \tag{3}$$

where χ is the strength of the interaction, and T is the temperature. The effect of a hard-core repulsion between all elements of the system is accounted for approximately by requiring that the system be incompressible. The grand canonical partition function of the system is[17]

$$\mathcal{Z} = \sum_{n_1,n_2} \frac{z_1^{n_1} z_2^{n_2}}{n_1! n_2!} \int \prod_{l=1}^{n_1} \tilde{\mathcal{D}}\mathbf{r}_{l,1} \prod_{m=1}^{n_2} \tilde{\mathcal{D}}\mathbf{r}_{m,2} \exp(-E/kT) \delta(\hat{\Phi}_h^{(1)} + \gamma_t \hat{\Phi}_t^{(1)} + \hat{\Phi}_h^{(2)} + \gamma_t \hat{\Phi}_t^{(2)} - 1). \tag{4}$$

The delta function in the above enforces the constraint of incompressibility. The notation $\int \tilde{\mathcal{D}}\mathbf{r}_{l,L}$ denotes a functional integral over the possible configurations of the l'th lipid of type L and in which, in addition to the Boltzmann weight, the path is weighted by the factor $\mathcal{P}[\mathbf{r}_{l,L}(s); 0, \alpha_L]$, with

$$\mathcal{P}[\mathbf{r}, s_1, s_2] = \mathcal{N} \exp\left[-\frac{1}{8R_g^2} \int_{s_1}^{s_2} ds \left|\frac{d\mathbf{r}(s)}{ds}\right|^2\right], \tag{5}$$

where $\mathcal{N}$ is an unimportant normalization constant and $R_g \equiv (Na^2/6)^{1/2}$ is the radius of gyration of a tail of length N.

We note that because of the choice of this weight function, $\mathcal{P}$, and the lack of any explicit interaction between chain segments to prevent their intersection, the behavior of the chains is Gaussian. This is appropriate because we view the chains as forming an incompressible melt. Under such conditions, a flexible, interacting, polymer chain behaves as an ideal, and therefore Gaussian, one[18,19]. It is not clear, of course, that an ideal *lipid* chain, which is certainly not flexible, can be treated as Gaussian. This approximation must overestimate the entropy of the tails, whose fewer thermally accessible configurations are presumably modelled more accurately by the Restricted Isomeric States Model[20,21]. But how serious is this overestimation, is also unclear. Ultimately the efficacy of our model in capturing the behavior of lipids can be judged only by a comparison with experiment. This was done for the lipid phase behavior in reference[15], and the comparison was very good. Even the variation with solvent concentration and with temperature of the characteristic period of the lamellar and hexagonal phases agreed very well. It is this

agreement with experiment of the calculated phase behavior which provides the support for applying the model to the calculation of other properties, such as the distribution of lipids in mixtures investigated here.

To proceed, we make the partition function of Eq. 4 more tractable by introducing into it the identity

$$\begin{aligned} 1 &= \int \mathcal{D}\Phi_h^{(L)} \delta(\Phi_h^{(L)} - \hat{\Phi}_h^{(L)}), \\ &= \int \mathcal{D}\Phi_h^{(L)} \mathcal{D}W_h^{(L)} \exp\left\{ \frac{1}{v_h} \int W_h^{(L)}(\mathbf{r})[\Phi_h^{(L)}(\mathbf{r}) - \hat{\Phi}_h^{(L)}(\mathbf{r})] d\mathbf{r} \right\}, \end{aligned} \tag{6}$$

where the integration on $W_h^{(L)}$ extends up the imaginary axis. We also insert such an identity for the density $\hat{\Phi}_t^{(L)}(\mathbf{r})$, and a similar representation for the delta function which enforces the incompressibility constraint. The partition function becomes

$$\mathcal{Z} = \int \mathcal{D}\Xi \prod_{L=1}^{2} \mathcal{D}\Phi_h^{(L)} \mathcal{D}W_h^{(L)} \mathcal{D}\Phi_t^{(L)} \mathcal{D}W_t^{(L)} \exp[-\Omega/kT], \tag{7}$$

where the grand potential Ω is given by

$$\begin{aligned} \Omega = -\frac{kT}{v_h} \sum_{L=1}^{2} \left\{ z_L \mathcal{Q}_L[W_h^{(L)}, W_t^{(L)}] + \int d\mathbf{r} \left[W_h^{(L)}(\mathbf{r}) \Phi_h^{(L)}(\mathbf{r}) + W_t^{(L)}(\mathbf{r}) \Phi_t^{(L)}(\mathbf{r}) \right] \right\} \\ + E[\Phi_h^{(1)} + \Phi_h^{(2)}, \Phi_t^{(1)} + \Phi_t^{(2)}] - \frac{kT}{v_h} \int d\mathbf{r}\, \Xi(\mathbf{r})(\Phi_h^{(1)}(\mathbf{r}) + \gamma_t \Phi_t^{(1)}(\mathbf{r}) + \Phi_h^{(2)}(\mathbf{r}) + \gamma_t \Phi_t^{(2)}(\mathbf{r}) - 1), \end{aligned} \tag{8}$$

and $\mathcal{Q}_L$ is the partition functions of a single lipid, of type L, in the external fields $W_h^{(L)}$ and $W_t^{(L)}$;

$$\mathcal{Q}_L = \int \tilde{\mathcal{D}}\mathbf{r}_L \exp\left\{ -W_h^{(L)}(\mathbf{r}_L(\alpha_L/2)) - \int_0^{\alpha_L} ds\; W_t^{(L)}(\mathbf{r}_L(s)) \right\}, \qquad L = 1, 2. \tag{9}$$

To this point, no approximations in the evaluation of the partition function of the model have been made, but it has been put in a form in which the self-consistent field (SCF) approximation appears naturally. The need for an approximation arises from the fact that the functional integrals in Eq. 7 over $W_h^{(L)}$ and $W_t^{(L)}$ cannot be carried out. The SCF consists in replacing the exact free energy, $-kT \ln \mathcal{Z}$ by the extremum of Ω. We denote the values of the $\Phi_h^{(L)}$, $W_h^{(L)}$, $\Phi_t^{(L)}$, $W_t^{(L)}$ and Ξ which extremize Ω by lower case letters. They are obtained from the following set of self consistent equations:

$$\phi_h^{(L)}(\mathbf{r}) = -z_L \frac{\delta \mathcal{Q}_L}{\delta w_h^{(L)}(\mathbf{r})}, \qquad L = 1, 2, \tag{10}$$

$$\phi_t^{(L)}(\mathbf{r}) = -z_L \frac{\delta \mathcal{Q}_L}{\delta w_t^{(L)}(\mathbf{r})}, \qquad L = 1, 2, \tag{11}$$

$$w_h^{(L)}(\mathbf{r}) = 2\chi N \sum_{L'} \phi_t^{(L')}(\mathbf{r}) - \xi(\mathbf{r}), \qquad L = 1, 2, \tag{12}$$

$$w_t^{(L)}(\mathbf{r}) = 2\chi N \sum_{L'} \phi_h^{(L')}(\mathbf{r}) - \gamma_t \xi(\mathbf{r}), \qquad L = 1, 2 \tag{13}$$

$$1 = \sum_{L} \phi_h^{(L)}(\mathbf{r}) + \gamma_t \sum_{L} \phi_t^{(L)}(\mathbf{r}). \tag{14}$$

Note that $w_h^{(1)} = w_h^{(2)}$ and $w_t^{(1)} = w_t^{(2)}$, so that henceforth we shall drop the superscripts on the fields w_h and w_t. It is convenient, further, to introduce the total headgroup and total tail densities

$$\phi_h(\mathbf{r}) = \phi_h^{(1)}(\mathbf{r}) + \phi_h^{(2)}(\mathbf{r}) \tag{15}$$

$$\phi_t(\mathbf{r}) = \phi_t^{(1)}(\mathbf{r}) + \phi_t^{(2)}(\mathbf{r}), \tag{16}$$

and to measure chemical potentails relative to that of lipid 1. This has the effect that $z_1 = 1$, and $z_2 = z$, the chemical potential of lipid 2 relative to that of 1. The free energy in this approximation, Ω_{scf} is

$$-\Omega_{scf} = \frac{kT}{v_h}\left[\sum_{L=1}^{2} z_L \mathcal{Q}_L[w_h, w_t] + \int d\mathbf{r}[w_h(\mathbf{r})\phi_h(\mathbf{r}) + w_t(\mathbf{r})\phi_t(\mathbf{r})]\right] - E[\phi_h, \phi_t], \tag{17}$$

$$= \frac{kT}{v_h}\sum_{L=1}^{2} z_L \mathcal{Q}_L[w_h, w_t] + E[\phi_h, \phi_t], \tag{18}$$

$$= kT(n_1 + n_2) + E[\phi_h, \phi_t], \tag{19}$$

with E given by Eq.3. There remains only the calculation of the partition function of the single lipid l of type L in the external fields w_h and w_t. One defines the end-segment distribution function

$$q^{(L)}(\mathbf{r}, s) = \int \mathcal{D}\mathbf{r}_l(s)\delta(\mathbf{r} - \mathbf{r}_l(s)) \exp\left\{-\int_0^s dt \left(\left[\frac{1}{8R_g^2}|\frac{d\mathbf{r}_l(t)}{dt}|^2\right] + w_h(\mathbf{r}_l(t))\delta(t - \alpha_L/2) + w_t(\mathbf{r}_l(t))\right)\right\}, \tag{20}$$

which satisfies the equation

$$\frac{\partial q^{(L)}(\mathbf{r}, s)}{\partial s} = 2R_g^2\nabla^2 q^{(L)}(\mathbf{r}, s) - [w_h(\mathbf{r})\delta(s - \alpha_L/2) + w_t(\mathbf{r})]q^{(L)}(\mathbf{r}, s), \tag{21}$$

with initial condition

$$q^{(L)}(\mathbf{r}, 0) = 1. \tag{22}$$

The partition functions of the two types of lipid are, then,

$$\mathcal{Q}_L = \int d\mathbf{r}\ q^{(L)}(\mathbf{r}, \alpha_L). \tag{23}$$

It then follows from Eqs. 10 and 11 that

$$\phi_h(\mathbf{r}) = \exp[-w_h(\mathbf{r})]\sum_{L=1}^{2} z_L q^{(L)}(\mathbf{r}, \frac{\alpha_L}{2}-)q^{(L)}(\mathbf{r}, \frac{\alpha_L}{2}-), \tag{24}$$

$$\phi_t(\mathbf{r}) = \sum_{L=1}^{2} z_L \int_0^{\alpha_L} ds\ q^{(L)}(\mathbf{r}, s)q^{(L)}(\mathbf{r}, \alpha_L - s),$$

$$= 2\sum_{L=1}^{2} z_L \int_0^{\alpha_L/2} ds\ q^{(L)}(\mathbf{r}, s)q^{(L)}(\mathbf{r}, \alpha_L - s), \tag{25}$$

where $z_1 = 1$ and $z_2 = z$. The self-consistent equations 10 to 14 can now be solved in real space. For the periodic phases in which we are interested, such as the lamellar, inverted hexagonal, gyroid, etc., it is more convenient to do so in Fourier space.

III. THEORY: FOURIER SPACE

Because the densities, fields, and end point distribution function depend only on a single coordinate, they reflect the space group symmetry of the ordered phase they describe. To make that symmetry manifest, we expand all functions of position in a complete, orthonormal, set of functions $f_i(\mathbf{r}), i = 1, 2, 3...$, which have the desired space group symmetry[22]; *e.g.*

$$\phi_h(\mathbf{r}) = \sum_i \phi_{h,i} f_i(\mathbf{r}), \tag{26}$$

$$\delta_{i,j} = \frac{1}{V}\int d\mathbf{r} f_i(\mathbf{r})f_j(\mathbf{r}), \tag{27}$$

where V is the volume of the system. Furthermore we choose the $f_i(\mathbf{r})$ to be eigenfunctions of the Laplacian

$$\nabla^2 f_i(\mathbf{r}) = -\frac{\lambda_i}{D^2} f_i(\mathbf{r}), \tag{28}$$

where D is a length scale for the phase. We set $f_1 = 1$. Expressions for the unnormalized basis functions for all space-group symmetries can be found in X-ray tables[23]. The self-consistent equations in Fourier space become

$$w_{h,i} = 2\chi N \phi_{t,i} - \xi_i, \tag{29}$$

$$w_{t,i} = 2\chi N \phi_{h,i} - \gamma_t \xi_i, \tag{30}$$

$$\delta_{i,1} = \phi_{h,i} + \gamma_t \phi_{t,i}. \tag{31}$$

To obtain the partition functions and densities, we proceed as follows. For any function $G(\mathbf{r})$, we can define a symmetric matrix

$$(G)_{ij} \equiv \frac{1}{V} \int f_i(\mathbf{r}) G(\mathbf{r}) f_j(\mathbf{r}) d\mathbf{r} \tag{32}$$

Note that $(G)_{1i} = (G)_{i1} = G_i$, the coefficient of $f_i(\mathbf{r})$ in the expansion of $G(\mathbf{r})$. Matrices corresponding to functions of $G(\mathbf{r})$, such as

$$\left(e^G\right)_{ij} \equiv \frac{1}{V} \int f_i(\mathbf{r}) e^{G(\mathbf{r})} f_j(\mathbf{r}) d\mathbf{r}, \tag{33}$$

are evaluated by making an orthogonal transformation which diagonalizes $(G)_{ij}$. The densities are obtained from the end point distribution function. After Fourier transforming the diffusion equation, Eq. 21, one readily obtains the solution

$$\begin{aligned} q_i^{(L)}(s) &= \left(e^{-As}\right)_{i,1}, \qquad \text{if } s < \alpha_L/2 \\ &= \sum_j \left(e^{-w_h}\right)_{ij} \left(e^{-\alpha_L A/2}\right)_{j,1}, \qquad s = \alpha_L/2 \\ &= \sum_{j,k} \left(e^{-A(s-\alpha_L/2)}\right)_{i,j} \left(e^{-w_h}\right)_{j,k} \left(e^{-\alpha_L A/2}\right)_{k,1}, \qquad s > \alpha_L/2, \end{aligned} \tag{34}$$

where the elements of the matrix A are given by

$$A_{i,j} = \frac{2R_g^2}{D^2} \lambda_i \delta_{ij} + (w_t)_{ij}. \tag{35}$$

From this, the Fourier amplitudes of the densities follow from eqs. 24 and 25;

$$\phi_{h;i} = \sum_{L=1}^{2} z_L \sum_{jkl} \left(e^{-w_h}\right)_{ij} \Gamma_{jkl} q_k^{(L)}(\frac{\alpha_L}{2}-) q_l^{(L)}(\frac{\alpha_L}{2}-), \tag{36}$$

$$\phi_{t;i} = 2 \sum_{L=1}^{2} z_L \int_0^{\alpha_L/2} ds \sum_{jk} \Gamma_{ijk} q_j^{(L)}(s) q_k^{(L)}(\alpha_L - s), \tag{37}$$

$$\tag{38}$$

with

$$\Gamma_{ijk} \equiv \frac{1}{V} \int f_i(\mathbf{r}) f_j(\mathbf{r}) f_k(\mathbf{r}). \tag{39}$$

The grand potential within the self-consistent field approximation, Eq 19, becomes

$$-\Omega_{scf} = \frac{kTV}{v_h} \left[\phi_{h,1} + 2\chi N \sum_i \phi_{h,i} \phi_{t,i} \right] \tag{40}$$

This free energy still depends on D, the length scale of the periodic phase, which must be determined by minimization of the free energy. After this is done, we compare the free energies obtained for phases of different space group symmetries, and thus obtain the phase diagram of the system.

The infinite set of self-consistent equations 29 to 37 must be truncated to be solved numerically, and we have employed up to 50 basis functions in our calculations for the lamellar, hexagonal, and b.c.c. phases, and 100 for the gyroid phases.

IV. RESULTS

A. Phase Diagrams

We begin by presenting, in Fig. 1, our results for the phase diagram of a single lipid with tails each of N units as a function of its architecture. We have defined an effective temperature, $T_N^* \equiv 1/2\chi N$. Note that T_N^* is length-dependent, i.e., the value of T_N^* differs for lipids of different length N even at the same physical temperature T. In our previous work[15], we found that for the system of dioleoylphosphatidylethanolamine a T_N^* of 0.06 corresponded to a physical temperature of approximately 20°C. The architecture is characterized by the volume of the head group relative to that of the entire lipid, $f \equiv v_h/(v_h + 2Nv_t)$. We have examined the common lipid phases, including the bi-continuous double-diamond phase (Pn3m), for stability, and found in addition to the lamellar phase only the normal and inverted versions of the body-centered cubic ($Im3m$), hexagonal, and gyroid $Ia3d$, phases to be stable. One sees that the diagram is quite reasonable and illustrates quantitatively the qualitative ideas of structure being driven by packing considerations[24].

We now turn to a mixture of two lipids. We have chosen $N_1 = N$ and $N_2 = 1.5N$ (i.e., $\alpha_1 = 1$, and $\alpha_2 = 1.5$) so that the extended length of the tails of lipid 2 are 1.5 times those of lipid 1. Further we have taken $\gamma_t \equiv 2N_1 v_t/v_h = 2.5$. With these parameters, the volume of the head group relative to that of the entire lipid is, for lipid 1, $f_1 \equiv 1/(1+\alpha_1\gamma_t) = 0.2857$, while that of lipid 2 is $f_2 \equiv 1/(1+\alpha_2\gamma_t) = 0.2105$. For comparison, the relative head group volume of dioleoylphosphatidylethanolamine calculated from volumes given in the literature[25] is $f = 0.254$. From the phase diagram of Fig. 1, one sees that lipid 1 forms a lamellar phase, while lipid 2 forms an inverted hexagonal, H_{II}, phase.

The phase diagram of the lipid mixture is shown in the solid lines of Fig. 2 as a function of the volume fraction of lipid 1, $\Theta \equiv \phi_h^{(1)} + \gamma_t \phi_t^{(1)}$ and the reduced temperature $T^* \equiv 1/2\chi N_1$. Here N_1 is a constant, the length of the tails of lipid 1, so that the definition of the temperature T^* is independent of the composition of the mixture as it should be. Small regions of body-centered cubic phase near the transition to the disordered phase have been ignored in the phase diagram. We are unaware of experimental phase diagrams from anhydrous mixtures of lamellar- and hexagonal-forming lipids with the same headgroup, as we have calculated here. However phase diagrams have been obtained for mixtures of lamellar-forming phosphatidylcholine and hexagonal-forming phosphatidylethanolamine. Those obtained for anhydrous mixtures of dilinoleoylphosphatidylethanolamine and palmitoyloleoylphosphatidylcholine[26], and for mixtures of dioleoylphosphatidylcholine and dioleoylphosphatidylethanolamine and 10% water by weight[27] are quite similar to Fig. 2 as they each show a significant region of cubic phase between the inverted hexagonal phase, which dominates at low concentrations of the lamellar-forming lipid, and the lamellar phase, which dominates at high concentration. We also observe that about 20% of one lipid added to the other is sufficient to bring about a change of phase, which is in accord with experiment[28]. Lastly, if the temperature is not too low, a decrease of the volume fraction of the lamellar-forming lipid causes the gyroid phase to be stable at increasing temperatures. Therefore the addition of longer non-lamellar lipids to the mixture stabilizes the non-lamellar phase, as in the experiment of Tate and Gruner[13].

We now show that there is a simple "effective single lipid" approximation by which one can obtain rather well the phase diagram of the mixture, Fig. 2, utilizing only the information from the phase diagram of the single lipid, Fig. 1. For this purpose, we must find a relationship between the coordinates (f, T_N^*) in Fig.1 and (Θ, T^*) in Fig. 2. Note that whereas the temperature scale T^* is independent of the composition of the mixture, the appropriate scale of Fig. 1 would vary from $T_{N_2}^* = T^*/1.5$ when the mixture contained lipid 2 only to $T_{N_1}^* = T^*$ at the other extreme.

To obtain the desired relationship, we first note that from the definitions of f and γ_t, it follows that $2Nv_t/v_h = (1-f)/f$ and $2N_1 v_t/v_h = \gamma_t$, from which one obtains $T_N^*/T^* = N_1/N = f\gamma_t/(1-f)$. Second, as f is defined as the volume fraction of the head group for a single lipid, it is natural to assume $f = \Theta f_1 + (1-\Theta)f_2$, the volume fraction of the head groups, in the mixture. Hence, in the "effective single lipid" approximation the coordinates of a point on the phase diagram of the mixture may be obtained from those of the single lipid according to

$$\Theta = \frac{f - f_2}{f_1 - f_2}, \tag{41}$$

$$T^* = \frac{1-f}{f\gamma_t} T_N^*. \tag{42}$$

The results of this "single effective lipid" approximation is shown by the open diamonds in Fig. 2. The approximation is obviously very good. Thus we can obtain very easily the phase diagram of any anhydrous mixture of our model lipids from the results for a single lipid, given in Fig. 1.

B. Distribution of Lipids

We now turn to the central results of this paper, which is the distribution of the different lipids in the various phases. It is convenient at the outset to define two local order parameters, $\psi(\mathbf{r})$ and $\zeta(\mathbf{r})$:

$$\psi(\mathbf{r}) = \psi^{(1)}(\mathbf{r}) + \psi^{(2)}(\mathbf{r}), \tag{43}$$

$$\psi^{(L)}(\mathbf{r}) \equiv \phi_h^{(L)}(\mathbf{r}) - \frac{\phi_t^{(L)}(\mathbf{r})}{\alpha_L}, \qquad L = 1, 2, \tag{44}$$

$$\zeta(\mathbf{r}) \equiv \frac{\phi_t^{(1)}(\mathbf{r})}{< \phi_t^{(1)}(\mathbf{r}) >} - \frac{\phi_t^{(2)}(\mathbf{r})}{< \phi_t^{(2)}(\mathbf{r}) >}. \tag{45}$$

Each order parameter, $\psi^{(L)}(\mathbf{r})$ measures the local difference in head and tail segments of type L normalized such that the integral of the order parameter over the unit cell vanishes. Thus $\psi(\mathbf{r})$ measures the local difference of all head and tail segments. It provides information on the separation of the lipid heads and tails. On the other hand, the order parameter $\zeta(\mathbf{r})$ measures the difference in local fractions of the tail segments belonging to the two different lipids. The brackets in its definitions denotes an average over some suitably defined tail region in which the order parameter $\psi(\mathbf{r})$ takes on negative values. For clarity, we employ somewhat different definitions of the tail region for the different phases. The average value of $\zeta(\mathbf{r})$ is zero over the defined tail region.

We begin with the lamellar phase and show in Fig. 3 the density profiles at a temperature $T^* = 0.0454$ and volume fraction of lipid 1, $\Theta = 0.6588$, a point very close to the phase boundaries between the lamellar phase and the inverted gyroid, G_{II}, phase. In Fig 3(a) we have plotted the volume fractions of the heads of lipids 1 and 2, $\phi_h^{(1)}$ and $\phi_h^{(2)}$, and the volume fractions of the tails, $\gamma_t \phi_t^{(1)}$, and $\gamma_t \phi_t^{(2)}$. Although the lamellar forming lipid 1 dominates, one can easily see that the density of lipid 1 tails decreases near the center of the lamellae by the order of 5 per cent from its maximum value of about 0.6. As the system is incompressible, this implies that the volume fraction of the tails of the non-lamellar forming lipid increases by about 8 per cent over the same range. To illustrate the *relative* difference in their volume fractions, we plot in Fig. 3(b) the order parameter $\zeta(x)$ where the tail region is defined here as $\psi(x) \leq 0$. Again one sees that the relative change in volume fractions is less than, but the order of 10 per cent, with the longer lipid 2 predominating in the center of the tail region. This comes about for two reasons. First, the tails of lipid 1 are shorter than those of lipid 2, so one expects there to be less lipid 1 near the center. Second, the effect of the temperature, which is to shorten the average end to end distance of the tails, is greater on the tails of lipid 1 than on the tails of lipid 2 because $T^*_{N_1} > T^*_{N_2}$. We have not plotted the relative variation of the head group volume fractions because it is so small, of the order of 0.5 per cent. Recall that all the head groups are identical.

We now turn to the inverted hexagonal, H_{II}, phase. We consider the system again at $T^* = 0.0454$ but now at volume fraction of lipid 1 of $\Theta = 0.27$ where the H_{II} and gyroid phases are almost in coexistence. In Fig. 4, we plot the order parameter $\psi(\mathbf{r})$. The dark regions correspond to positive values of the order parameter where the head groups dominate and the lighter regions where the tails dominate. The maximum value is 0.719 and the minimum value -0.286. Each gradation represents a change of 10 per cent. To make manifest the difference in densities of the tails from each lipid, we again look at the order parameter $\zeta(\mathbf{r})$ which is shown in Fig. 5. Here the tail region we have averaged over is the locus of points for which the order parameter $\psi(\mathbf{r}) \leq -0.282$. Regions with $\psi(\mathbf{r}) > -0.282$ are simply shown in white. Again the darker regions correspond to positive values of this order parameter where the tails of the lamellar forming lipid are relatively more probable to be found, while the lighter regions denote negative values where the non-lamellar forming lipid is more probable. One see that the latter lipid is more likely to be found in the next-nearest neighbor direction, in the region which is most difficult for the tails to fill. The maximum value of $\zeta(\mathbf{r})$ is 0.0352, and the minimum value is -0.0377 indicating that the relative volume fractions vary by the order of 3 per cent over the tail region. To make the variation in densities even clearer, we plot in Fig. 6(a) and 6(b) the volume fractions of the tails of the lipids as measured along the boundary of the Brillouin zone with the angle $\theta = 0$ corresponding to the direction of the nearest neighbors, and $\theta_0 = \pi/6$ corresponding to the direction of the next nearest neighbors. One sees that the density of the minority lamellar forming lipid is reduced by about 2 per cent in the next-nearest neighbor direction, while that of the majority non-lamellar forming lipid is is increased by about 0.6 per cent. Again, the variation with direction of the density of head groups is negligible.

In order to compare these densities changes with the curvature of the inverted hexagonal phase, we plot in Fig. 6(c) the mean curvature along the locus of points defined by $\psi(\mathbf{r}) = 0$, *i.e.*, on the curve on which the difference in volume fractions of all heads and tails vanishes. The mean curvature as a function of angle is well fit by

$$H(\theta) = H_0 + \sum_{n=1}^{5} H_n \cos(6n\theta), \tag{46}$$

with $H_0 = 1.55800$, $H_1 = -3.33 \times 10^{-3}$, $H_2 = 3.2 \times 10^{-4}$, $H_3 = -5.3 \times 10^{-4}$,$H_4 = 3.59 \times 10^{-3}$, and $H_5 = -8.2 \times 10^{-4}$. One see that the variation in the mean curvature is an order of magnitude smaller than that of the variation of the tails of the minority lipid, and also smaller than that of the majority lipid. There is also much more structure in the mean curvature. It is not surprising that this structure near the region where the head groups and tails meet is washed out in the region of the other end of the tails.

We now consider the inverted gyroid phase. We show in Fig. 7 and 8 two views of this phase at $T^* = 0.045$ and $\Theta = 0.4921$. The phase consists of two sublattices of tubes filled for the most part with head groups. The sublattices are related by mirror reflection. We have chosen to plot the surfaces defined by the order parameter $\psi(\mathbf{r}) = 0.5$ rather than $\psi(\mathbf{r}) = 0$ for in the latter case the tubes are much more difficult to recognize. Fig. 7 shows a view along the [001] direction while Fig. 8 is viewed from point (0.9,-2.4,2). These figures define the coordinate system which we use and show a cubic cell of side unity. Were the tubes shrunk to lines, three such lines would meet at nodes, and there would be 16 such nodes in the unit cell shown.

We wish to show what the relative densities of the two lipids are at the positions which are the easiest for the tails to fill, and those which are the most difficult for the tails to fill. These correspond to the points midway between nearest neighbors and next-nearest neighbors in the H_{II} phase. These positions are not obvious in the gyroid phase, but can be calculated. An example of a longest distance is shown in Fig. 8 by a solid line. The coordinates of the point shown, which is furtherest from any tube, is $(1/2, 3/16, 5/8)$ while the points on the tube centers closest to it are $(15/32, 7/32, 7/8)$ and $(17/32, 7/32, 3/8)$. Thus this longest distance is $d_{long} = (66)^{1/2}/32$. The shortest distances link two three-fold coordinated sites on the different sublattice, and one such shortest distance is shown in Fig. 8 by a dotted line. Two particular points on the tube centers connected by this distance and which are shown in the figure have the coordinates $(5/8, 3/8, 7/8)$ and $(7/8, 1/8, 5/8)$. The distance between these points is twice the shortest distance between a point midway between tubes and the tube centers themselves, and is therefore $d_{short} = 3^{1/2}/8$. Interestingly, the ratio of longest to shortest distances in the gyroid phase $d_{long}/d_{short} = (33/8)^{1/2}/(3)^{1/2}$ is only about 2 per cent larger than the corresponding ratio in the hexagonal and b.c.c. phases which is $2/(3)^{1/2}$ in both cases. At the temperature and composition selected, we find that at the point nearest to neighboring tubes and which requires the least stretching of the lipid tails, the volume fraction of the tails of the lamellar forming lipid 1 is $\gamma_t \phi_t^{(1)} = 0.448$ and that of the non-lamellar forming lipid 2 is $\gamma_t \phi_t^{(2)} = 0.537$. At the position requiring the most stretching of the tails, we find the volume fraction of the tails of lipid 1 has decreased to 0.431, while that of the longer lipid 2 has increased to 0.561.

In Fig. 9 the order parameter $\zeta(\mathbf{r})$, which shows the relative difference between the volume fractions of the tails of lipid 1 and lipid 2, is shown in a cut through the gyroid taken in the $[1\bar{1}0]$ direction and which passes through two points, $(-1/8, -1/8, -1/8)$ and $(1/8, 1/8, 1/8)$, which require the least stretch. Only the portion of the tail region defined by $\psi(\mathbf{r}) \leq -0.2$ is shown with any gray scale variation. The solid line connects the tube centers which lie closest to one another. The point midway along this line is that most easily reached by the lipid tails. The fact that the region around this point is dark indicates that the shorter lipid 1 is relatively more probable here. The maximum (black) and minimum values (white) of $\zeta(\mathbf{r})$ are 9.26×10^{-2} and -6.64×10^{-2} indicating a variation of relative volume fraction in the tail region shown which is on the order of 8 per cent. Figure 10 shows a cut in the [801] direction which passes through the point which is furtherest from the center of any tube. Again the region shown in gray scale variation is the tail region defined by $\psi(\mathbf{r}) \leq -0.2$. The maximum and minimum values of $\zeta(\mathbf{r})$ are 10.35×10^{-2} and -6.99×10^{-2} indicating a similar variation in volume fraction. The point at the center of the bent dark line is furtherest from the center of any tube. The black line ends on the centers of the two tubes closest to it. The lightest part of the generally dark tail region is very close to the point furtherest from any tube center and indicates that the relative probability of finding the tails of the non-lamellar forming lipid is large there. That the lightest part does not correspond exactly to the point furtherest from the tube center is probably due to the fact that this point is not necessarily the furtherest from the head-tail interface, and thus not necessarily the most difficult for the tails to reach, although it is probably quite close to being so.

In Fig. 11 we show the surface defined by the order parameter $\psi(\mathbf{r}) = -0.2$ in the region of the three-fold connectors. On that surface the order parameter $\zeta(\mathbf{r})$ is plotted. The largest value, which is black and at the center of this region, is 3.25×10^{-2} showing that the lamellar-forming lipids are more probable there. The smallest value, shown in the lightest gray, is -1.82×10^{-2} indicating a few per cent variation in this region. For comparison, the mean curvature on the surface defined by $\psi(\mathbf{r}) = 0$ is plotted in Fig. 12. The smallest value of the mean curvature, 0.20, occurs at the center, while the largest values, 0.52, occur away from it. As in the inverted hexagonal phase, one sees that the preferential location of the lamellar-forming lipids is at low curvature sites. Further there is more structure in the plot of the curvature on a surface near where the heads and tails meet than in the plot of the distribution of tail volume fractions deep within the tail region. That the region near the center of these three-fold connectors is characterized by small mean curvature is analogous to the results obtained by Matsen[29] for the gyroid phase of block copolymers. We used two hundred basis functions for this plot.

In sum, we have employed a lipid model which has given excellent results previously[15] for the phase diagram of dioleoylphosphatidyethanolamine in order to examine the distribution of tails in a mixture of lamellar forming and non-lamellar forming lipids. The two lipids are characterized by the same head group, but tails of different length. We have shown, both in the inverted hexagonal and gyroid phases, that the tails of the non-lamellar forming lipid are found preferentially in regions of the unit cell which are difficult to fill, and those of the lamellar forming lipid are found in the regions most easily filled. The variation in volume fraction is of the order of 1 to 10 per cent. The difference in lipid tail density is also correlated with the curvature of the surface which, loosely, separates the head groups from the tails although the former shows much less structure than the latter. It will be most interesting to apply this model to stalk-like structures thought to be of importance in membrane fusion to determine by what amount the presence of non-lamellar forming lipids can lower the free energy barrier to their formation[8]. This work was supported in part by the National Science Foundation under grant number DMR9876864.

---

[1] P.R. Cullis, M.J. Hope, B. de Kruijff, A.J. Verkleij, and C.P.S. Tilcock, in *Phopholipids and Cellular Regulation*, vol. 1, J.F. Kuo ed., (CRC Press, Boca Raton 1985) p1.

[2] de Kruijff, B., *Current Opinion in Chemical Biology*, 1, 564 (1997).

[3] An excellent introduction is provided by *Current topics in membranes* vol. 44, R. Epand ed. (Academic, San Diego, 1997).

[4] S. Morein, A. Andersson, L. Rilfors, and G. Lindblom, *J. Biol. Chem.* **271** 6801 (1996).

[5] D. Marsh, *Biochim Biophys Acta* **1286** 183 (1996).

[6] A.G. Rietveld, A.J. Verkleij, and B. de Kruijff *Biochim Biophys Acta* **1324** 262 (1997).

[7] V.S. Markin, M.M. Kozlov, V.L. Borovjagin, *Gen. Physiol. Biophys.* **5** 361 (1984).

[8] D.P. Siegel, *Biophysical J.* **65** 2124 (1993).

[9] L. Chernomordik, M.M. Kozlov, and J. Zimmerberg, *J. Membrane Biol.* **146** 1 (1995).

[10] L.V. Chernomordik and J. Zimmerberg, *Current Opinion in Structural Biology* **5** 541 (1995).

[11] G.L. Kirk and S.M. Gruner, *J. Phys. (Les Ulis,Fr.)* **46** 761 (1985).

[12] M.W. Matsen, *Macromolecules* **28** 5765 (1995).

[13] M.W. Tate and S.M. Gruner, *Biochemistry* **26** 231 (1987).

[14] S. Leibler and D.A. Andelman, *J. Phys.* (France) **48**, 2013 (1987).

[15] X.-j. Li and M. Schick, *Biophysical J.* (in press).

[16] J.M. Seddon, G. Cevc. and D. Marsh, *Biochemistry* **22**, 1280 (1983).

[17] M.W. Matsen, *Phys. Rev. Lett.* **74**, 4225 (1995).

[18] S.F. Edwards, *Proc. Phys. Soc.* **88** 265 (1966).

[19] S.F. Edwards, *J. Phys.* **A8**, 1670 (1975).

[20] P.J. Flory, *Statistical Mechanics of Chain Molecules* (Wiley-Interscience, New York, 1969).

[21] M. Müller and M. Schick, *Phys. Rev* **E57** 6973 (1998).

[22] M.W. Matsen and M. Schick, *Phys. Rev. Lett.* **72** 2660 (1994).

[23] N.F.M. Henry and K. Lonsdale (eds.), *International Tables for X-ray Crystallography* (Kynoch, Birmingham, 1969).

[24] J.N. Israelachvili, *Intermolecular and Surface Forces* (Academic, San Diego, 1985).

[25] R.P. Rand and N.L. Fuller, *Biophysical J.* **66** 2127 (1994).

[26] L.T. Boni and S.W. Hui, *Biochim Biophys Acta* **731** 177 (1983).

[27] P.-O. Eriksson, L.Rilfors, G. Lindblom, and G. Arvidson, *Chemistry and Physics of Lipids* **37** 357 (1985).

[28] C.P.S. Tilcock, M.B. Bally, S.B. Farren, and P.R. Cullis, *Biochemistry* **21** 4596 (1982).

[29] M.W. Matsen and F.S. Bates, *Macromolecules* **29** 7641 (1996).

Figure 1. Phase diagram of an anhydrous system of lipids as a function of the temperature T_N^* and the volume of the head group relative to that of the entire lipid, $f \equiv v_n/(v_n + 2Nv_t) = 1/(1+\gamma_t)$. In addition to the disordered (D) and lamellar L_α phases, there are body-centered cubic (bcc), hexagonal (H), and gyroid G phases. The subscripts I and II denote normal and inverted phases respectively. The dashed lines indicate extrapolated boundaries.

Figure 2. Phase diagram of a mixture of two lipids with the same head group, but one with tails 1.5 times the length of the other. Lipid 1, a lamellar-forming lipid, is characterized by $1/(1+\gamma_t) = 0.2857$ while the non-lamellar forming lipid 2, with the longer tails, is characterized by $1/(1+1.5\gamma_t) = 0.2105$. $T^* = 1/2\chi N_1$ is a measure of the temperature, and Θ is the volume fraction of lipid 1. Solid lines result from the full self-consistent field calculation of the mixture, while open diamonds result from the single effective lipid approximation. Very small regions of b.c.c phases have been ignored.

Figure 3. (a) Volume fractions of the head groups $\phi_h^{(1)}$ and $\phi_h^{(2)}$ of lipids 1 and 2 and of the tail groups $\gamma_t\phi_h^{(1)}$ and $\gamma_t\phi_h^{(2)}$ in the lamellar phase at $T^* = 0.045$ and volume fraction of lipid 1 $\Theta = 0.6588$.

(b) The order parameter $\zeta(x) \equiv \phi_t^{(1)}(x)/ < \phi_t^{(1)}(x) > -\phi_t^{(2)}(x)/ < \phi_t^{(2)}(x) >$, where the averages are taken over the region $\psi(x) \leq 0$.

Figure 4. The order parameter $\psi(\mathbf{r}) = \phi_h^{(1)}(\mathbf{r}) - \phi_t^{(1)}(\mathbf{r}) + \phi_h^{(2)}(\mathbf{r}) - (1/\alpha_2)\phi_t^{(2)}(\mathbf{r})$ in the H_{II} phase at $T^* = 0.045$ and $\Theta = 0.27$. The maximum value is 0.719 and the minimum value -0.286. Each gradation represents a change of 10 per cent.

Figure 5. The order parameter $\zeta(\mathbf{r})$ in the hexagonal phase of Fig. 4. The averages are taken over the region $\psi(\mathbf{r}) \leq -0.282$. Regions with $\psi(\mathbf{r}) > -0.282$ are shown in white. Light parts of the tail region indicate an excess of non-lamellar forming lipids, while darker areas represent excess of lamellar-forming lipids.

Figure 6. (a) Volume fraction of non-lamellar forming lipid 2 evaluated on the Brillouin zone edge from nearest-neighbor direction, $\theta = 0$, to next-nearest-neighbor direction, $\theta = \pi/6$.

(b) Volume fraction of lamellar forming lipid 1 evaluated on the Brillouin zone edge.

(c) Mean curvature of the surface defined by $\psi(\mathbf{r}) = 0$.

Figure 7. A view of the gyroid taken along the [001] direction. The surface is defined by the value of the order parameter $\psi(\mathbf{r}) = 0.5$ which is well within the region in which the head groups dominate.

Figure 8. A second view of the gyroid surface, defined as in Fig. 7. The longest distance between a point in the tail region and the axis of any tube is shown by two intersecting solid lines. The shortest distance between the axes of two tubes is shown by a dotted line. Such a line connects nearby regions of three-fold symmetry on the two different sublattices.

Figure 9. Order parameter $\zeta(\mathbf{r})$ shown in a cut which passes through the point requiring the least stretch of the lipid tails. The points closest together are shown connected by a solid line. The volume fractions of the tails are averaged over the region defined by $\psi(\mathbf{r}) \leq -0.2$. The region in which $\psi(\mathbf{r}) > -0.2$ is shown in white. The maximum value of $\zeta(\mathbf{r})$, in black, is 9.26×10^{-2} and the minimum value is -6.64×10^{-2}.

Figure 10. Order parameter $\zeta(\mathbf{r})$ shown in a cut which passes through the point furtherest from the axis of any tube. The volume fractions of the tails are averaged over the region defined by $\psi(\mathbf{r}) \leq -0.2$.The maximum value of ζ is 10.35×10^{-2} and the minimum is -6.99×10^{-2}.

Figure 11. The order parameter $\zeta(\mathbf{r})$ is plotted on the surface defined by the order parameter $\psi(\mathbf{r}) = -0.2$ in the region of the three-fold connectors. The largest value, which is black and at the center of this region, is 3.25×10^{-2} showing that the lamellar-forming lipids are more probable there. The smallest value, shown in the lightest gray, is -1.82×10^{-2} indicating a few per cent variation in this region.

Figure 12. The mean curvature on the surface defined by $\psi(\mathbf{r}) = 0$ is shown. The smallest value of the mean curvature, 0.20, occurs at the center, while the largest values, 0.52, occur away from it.

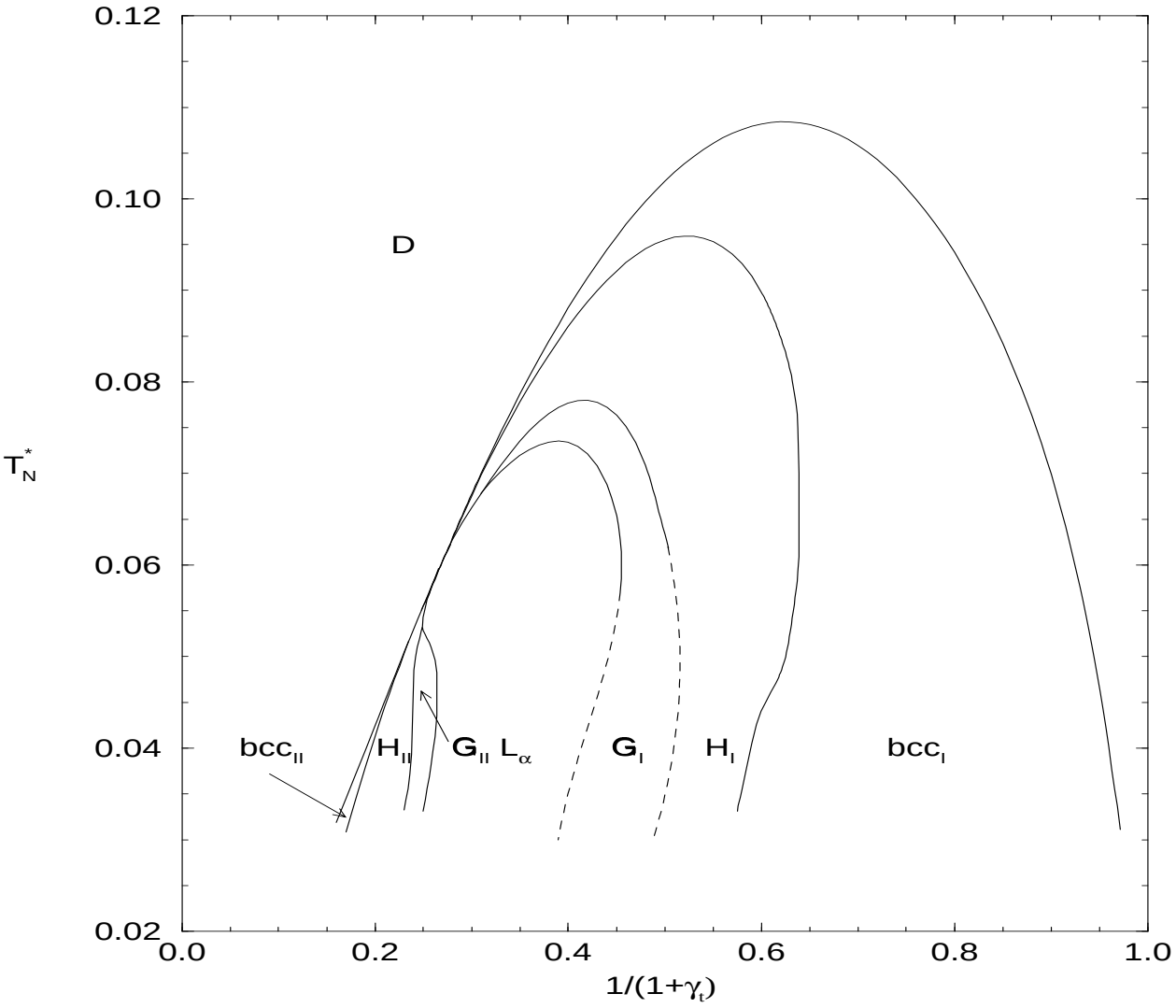
0.12
0.10
0.08
0.06
0.04
0.02
T_N^*
D
bcc_{II}
H_{II}
G_{II} L_α
G_I
H_I
bcc_I
0.0
0.2
0.4
0.6
0.8
1.0
$1/(1+\gamma_t)$

FIG. 1.

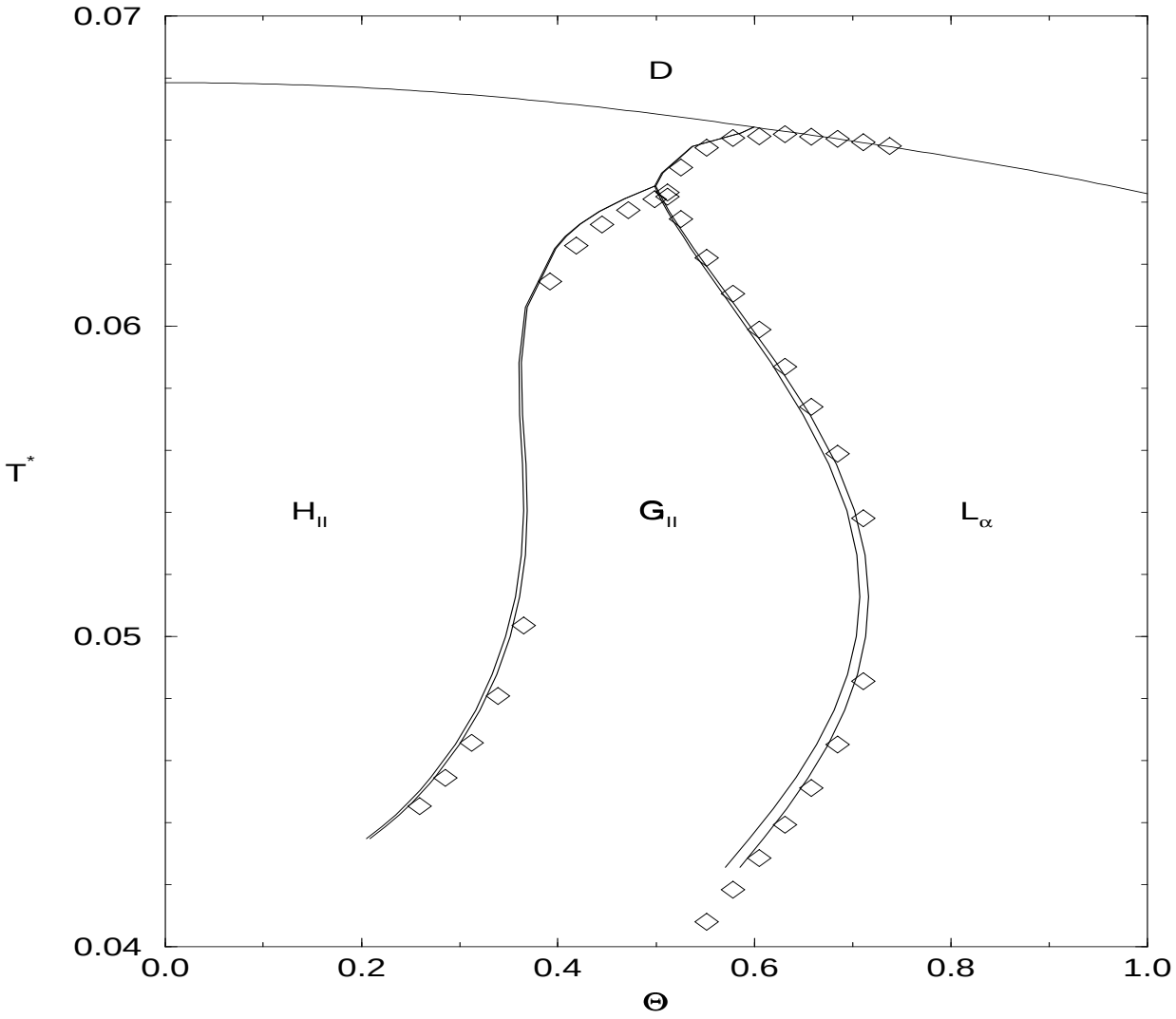

FIG. 2.

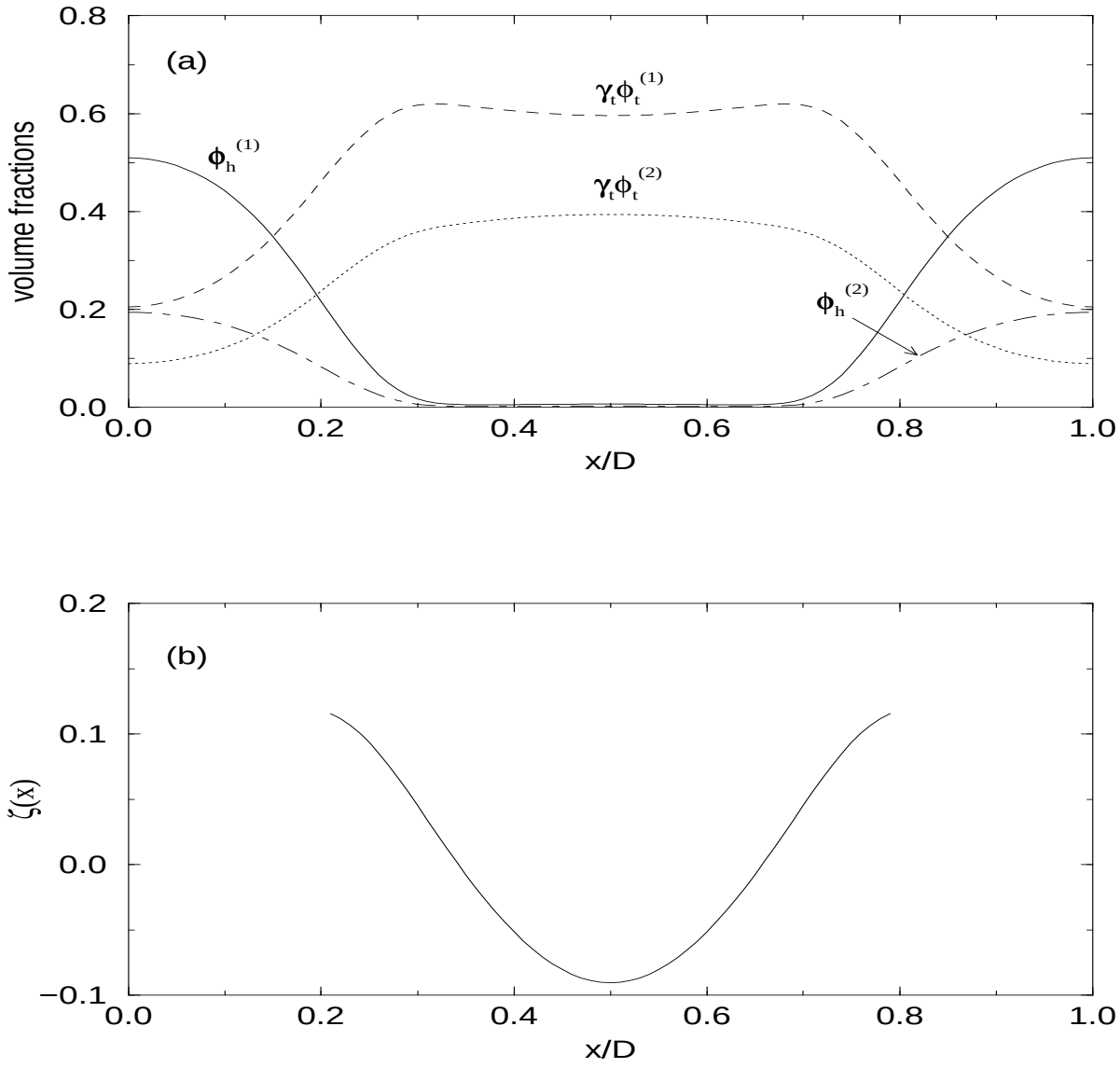
(a)
volume fractions
$\gamma_t\phi_t^{(1)}$
$\phi_h^{(1)}$
$\gamma_t\phi_t^{(2)}$
$\phi_h^{(2)}$
0.0
0.2
0.4
0.6
0.8
1.0
x/D

(b)
ζ(x)
0.2
0.1
0.0
−0.1
0.0
0.2
0.4
0.6
0.8
1.0
x/D

FIG. 3.

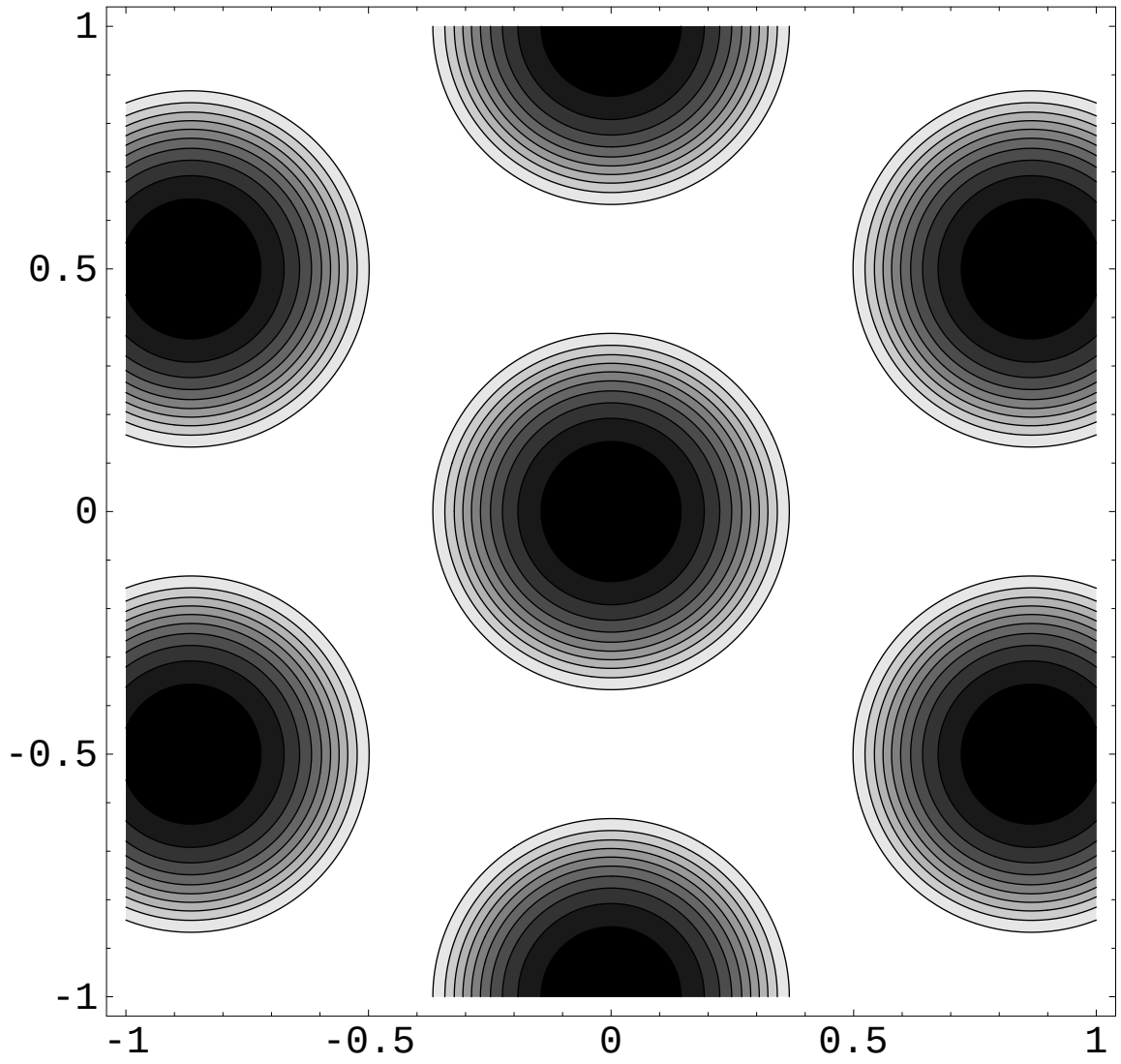

FIG. 4.

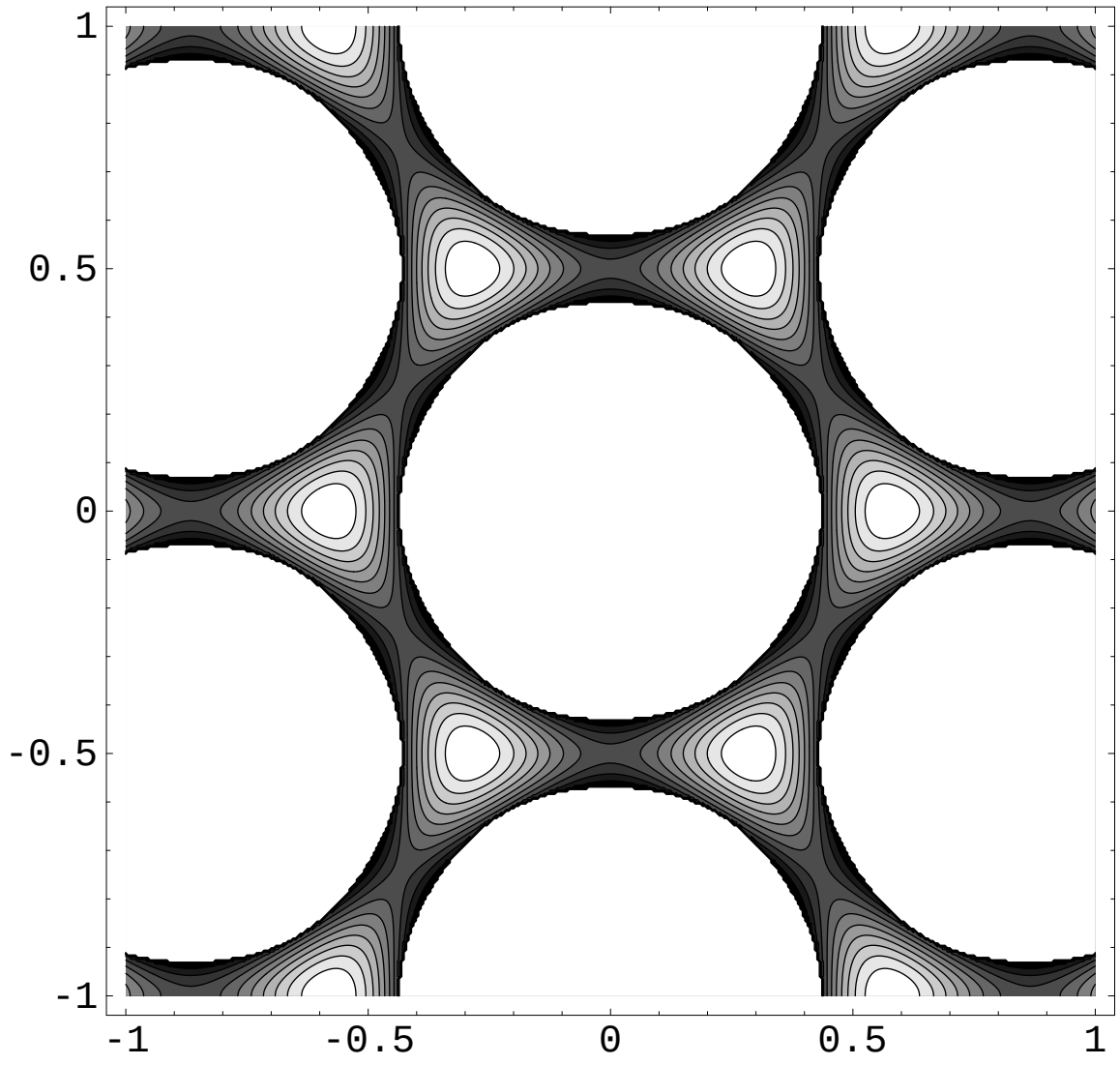

FIG. 5.

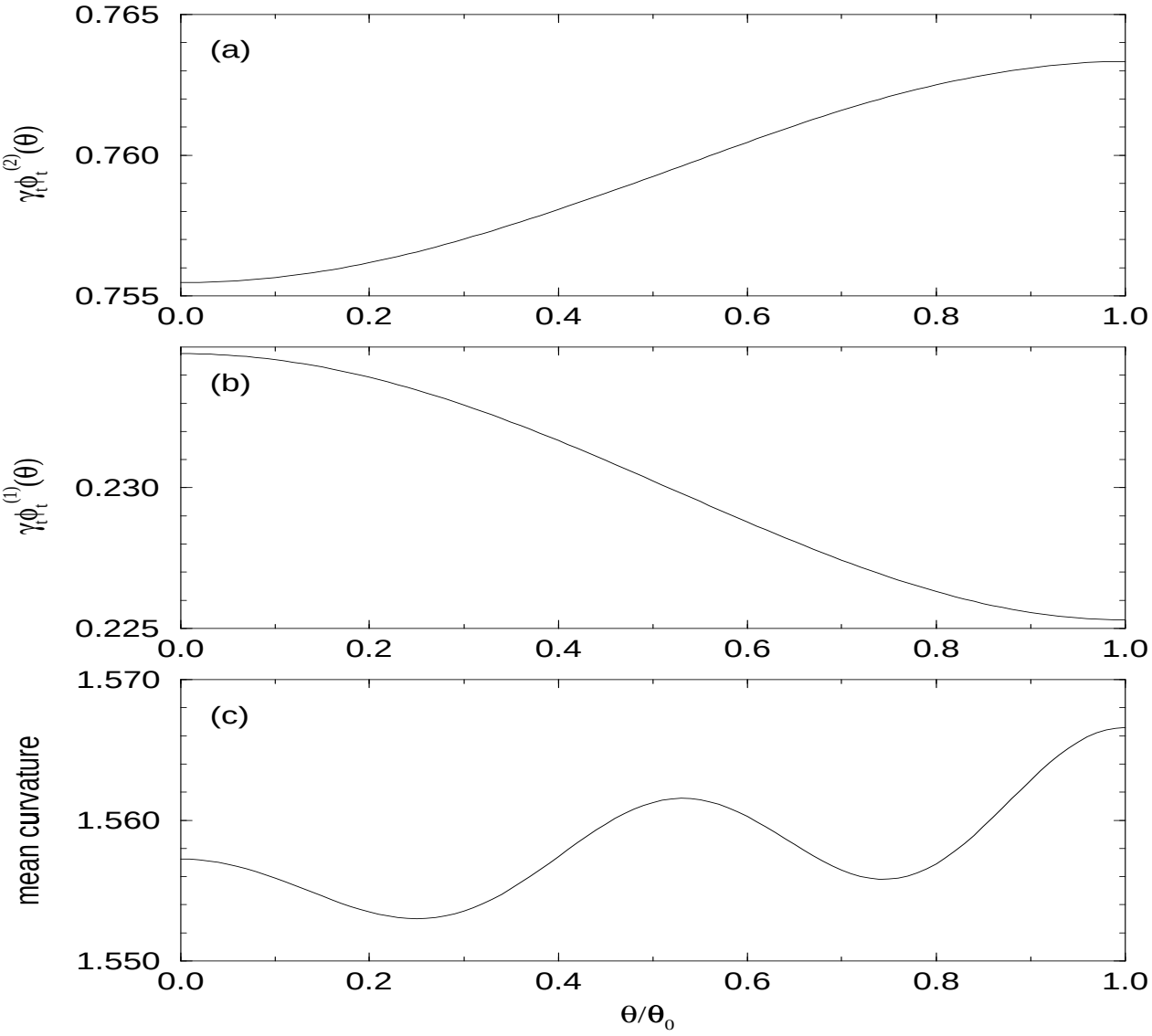
(a)
(b)
(c)
0.765
0.760
0.755
0.230
0.225
1.570
1.560
1.550
0.0
0.2
0.4
0.6
0.8
1.0
$\gamma\phi_{t't}^{(2)}(\theta)$
$\gamma\phi_{t't}^{(1)}(\theta)$
mean curvature
θ/θ_0

FIG. 6.

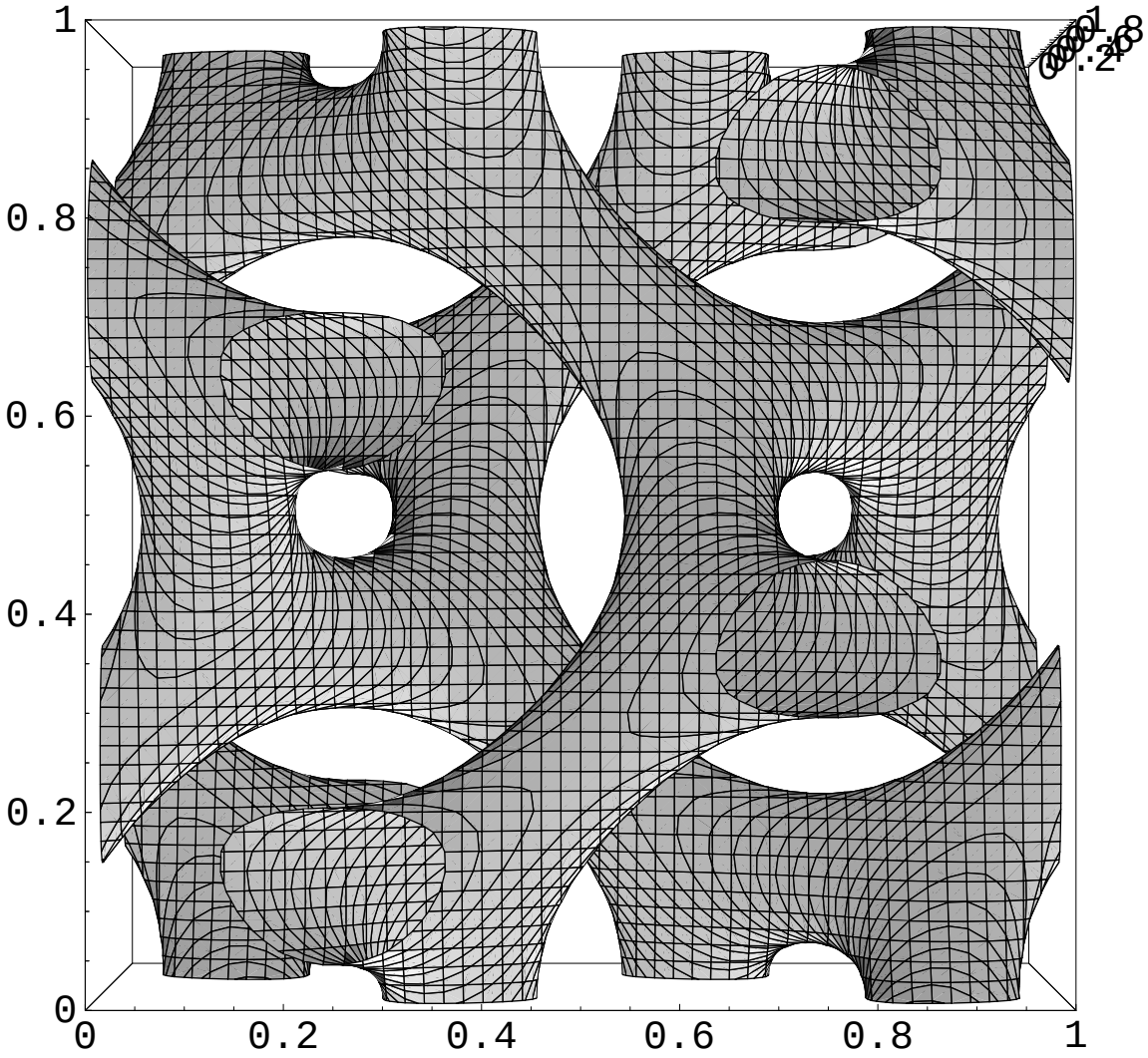

FIG. 7.

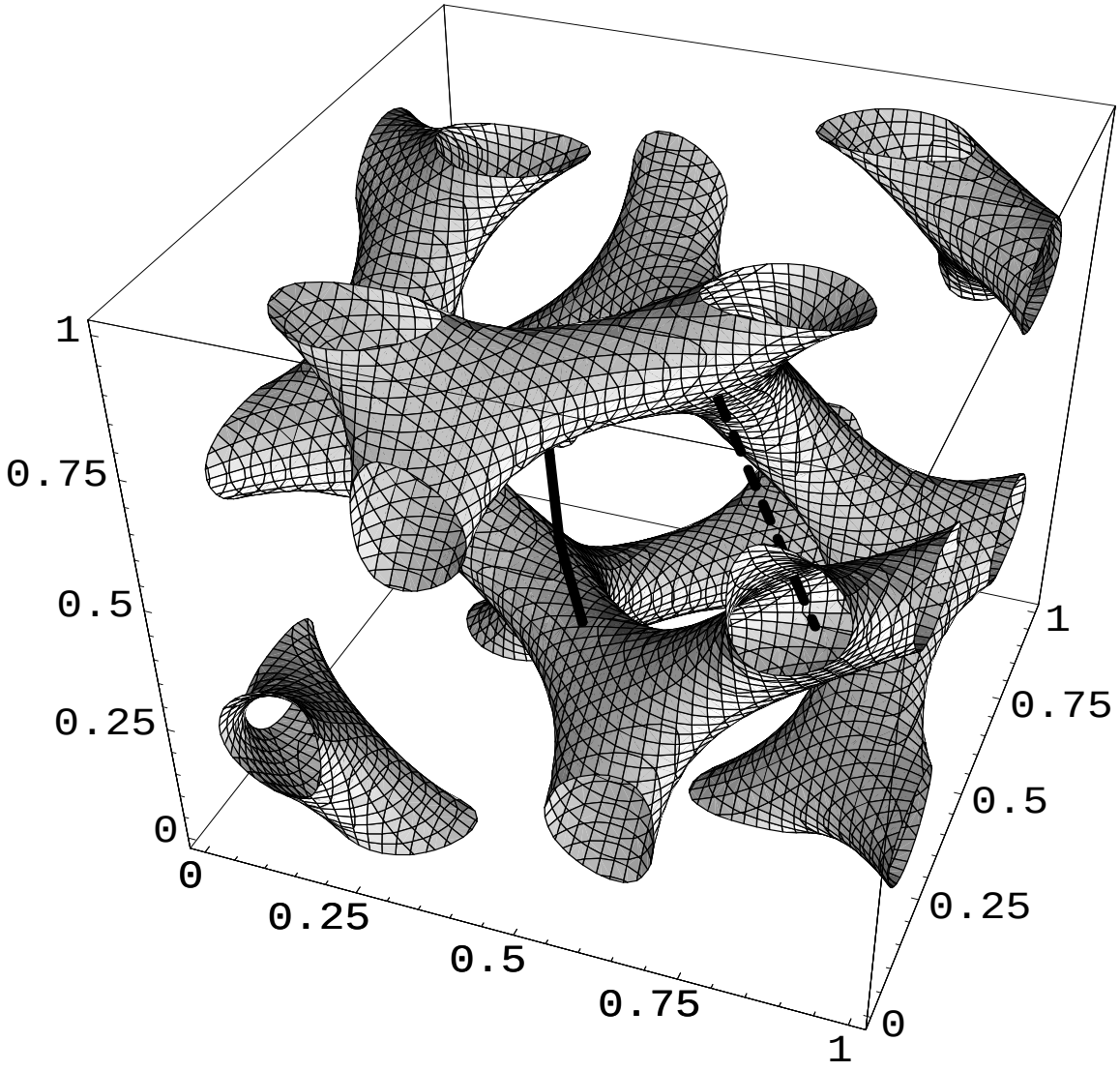

FIG. 8.

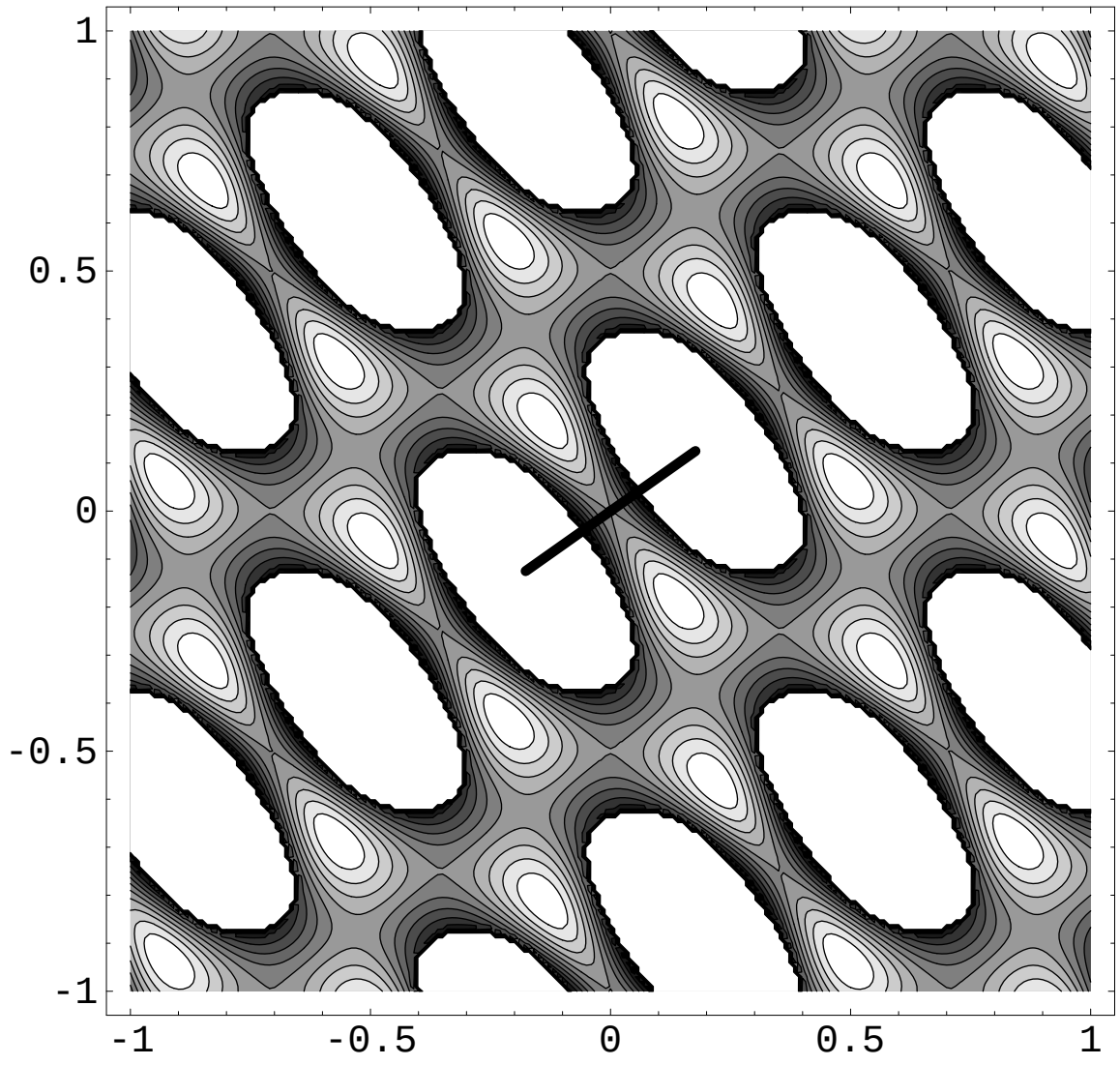

FIG. 9.

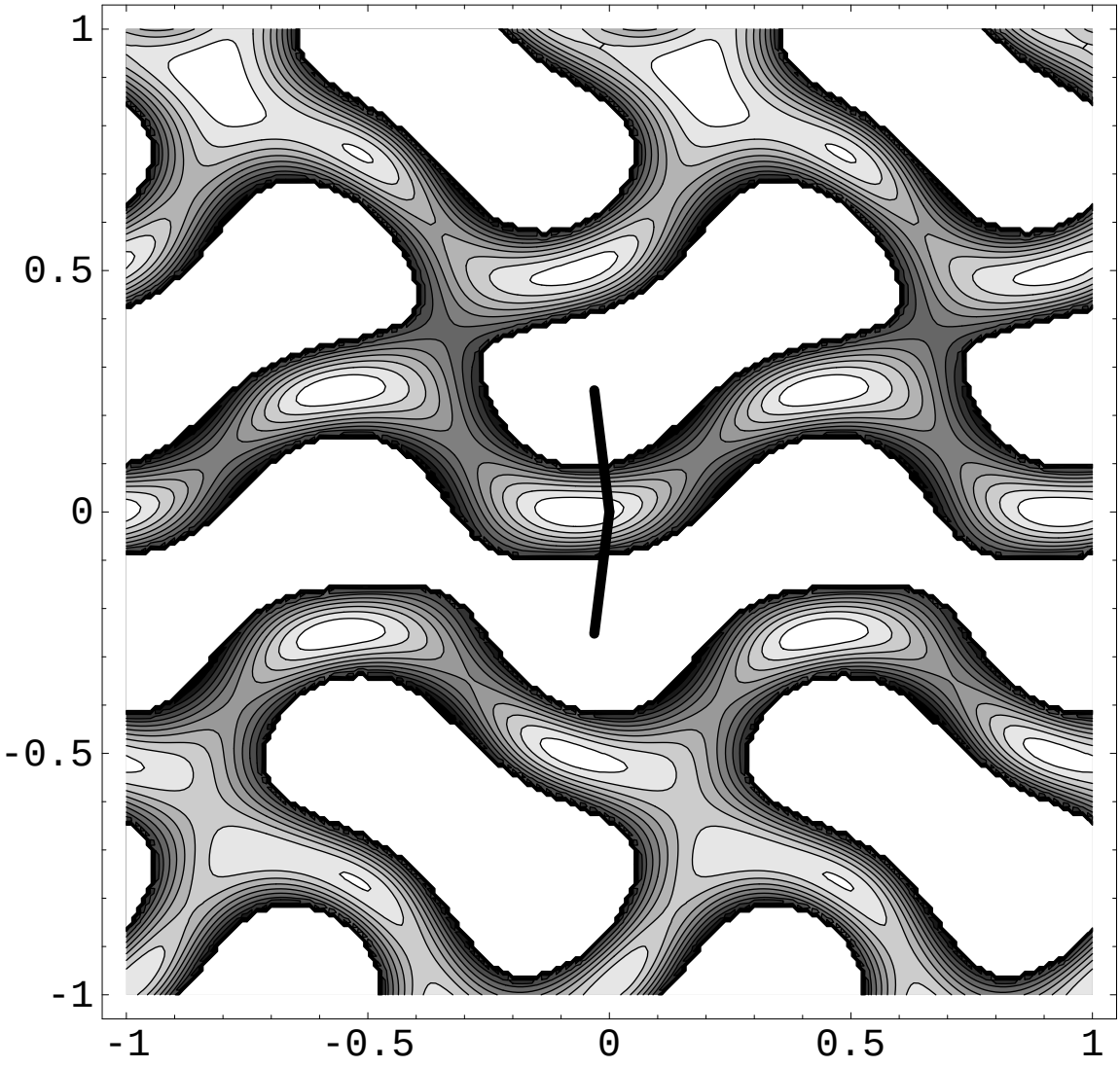

FIG. 10.

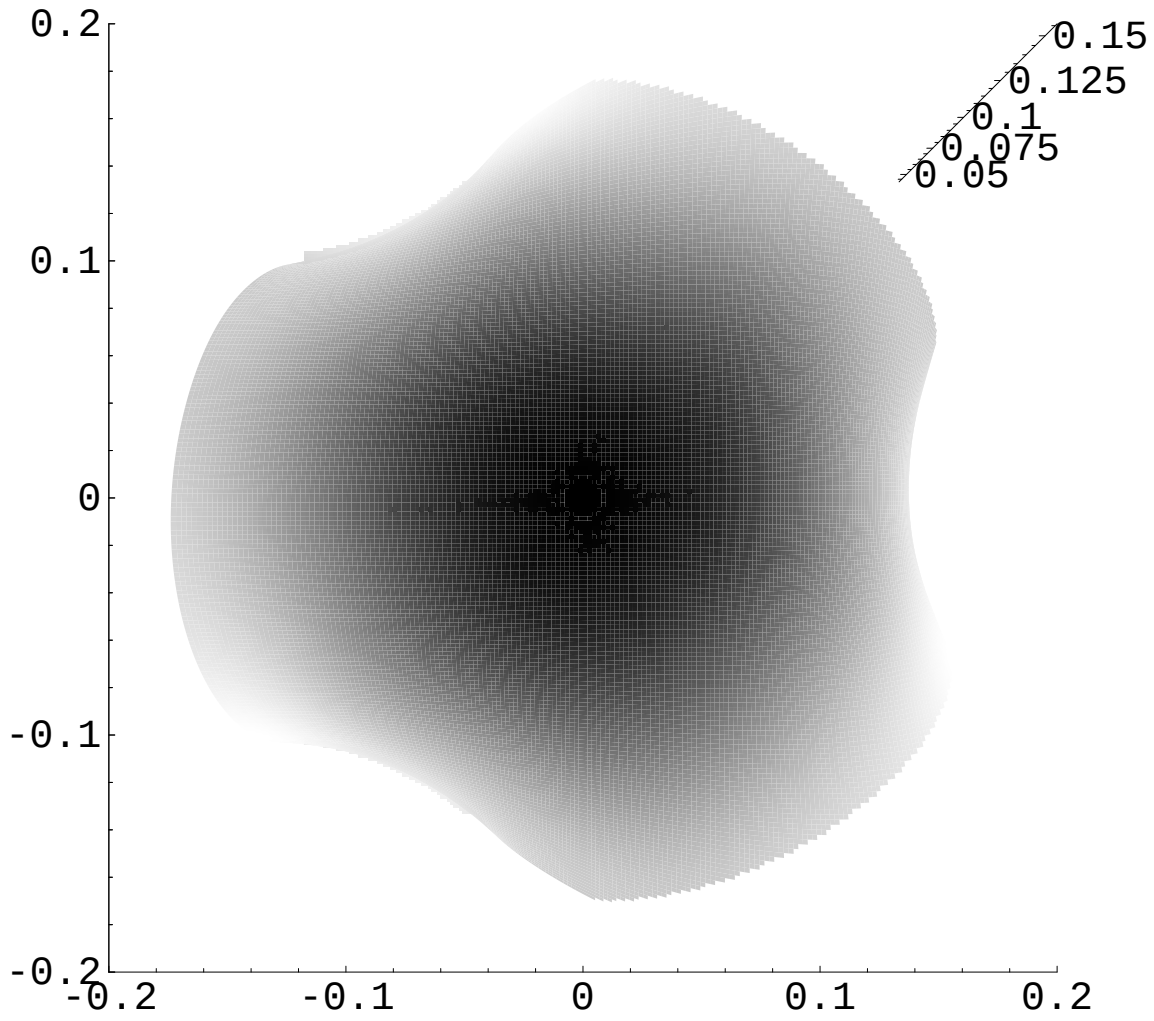

FIG. 11.

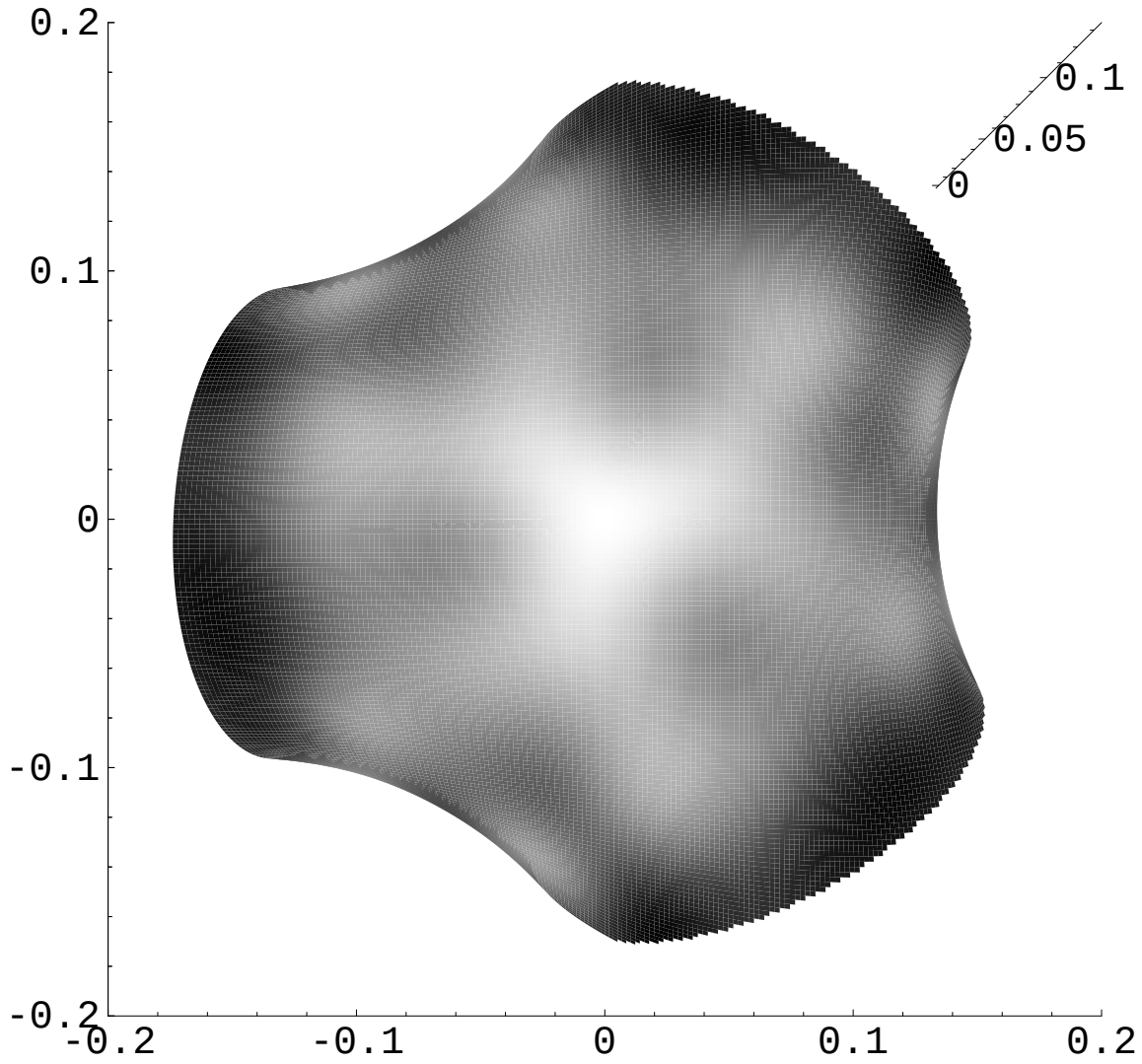

FIG. 12.